International Journal of Hydrogen Energy 142 (2025) 1196–1210

Contents lists available at ScienceDirect

International Journal of Hydrogen Energy

journal homepage: www.elsevier.com/locate/he

Feasible route towards decarbonising marine transport with flexible, hydrogen – enriched, reactivity controlled compression ignition mid-speed engines

Aneesh Vasudev [a,*], Amir Soleimani [a], Jari Hyvönen [b], Maciej Mikulski [a,**]

[a] Efficient Powertrain Solutions, School of Technology and Innovation, University of Vaasa, Wolffintie 34, Vaasa, FI-65200, Finland
[b] Wärtsilä Finland Oy, Teollisuuskatu 1, Vaasa, FI-65170, Finland

ARTICLE INFO

Handling Editor: Ibrahim Dincer

Keywords:
Multizone model
RCCI
H2 blending
Engine rapid prototyping

ABSTRACT

Hydrogen (H_2) admixing in Reactivity Controlled Compression Ignition (RCCI) technology engines is touted to enhance indicated efficiency (ITE>50%), optimize combustion and reduce greenhouse gas emissions. However, many pending issues remain regarding engine durability, nitrogen oxide (NO_X) emissions and blending limits. These issues are addressed by employing a novel performance-oriented model which simulates under 3 min, combustion physics with similar predictivity (>95% accuracy) as computational fluid dynamic results. This so-called multizone model is parameterized to real-world operating cycles from a dual-fuel mid-speed marine engine. By considering port-fuel injected H_2, the simulations show that combustion phasing advances at an average rate of 0.3°CA/% H_2, accompanied by a peak reduction in methane slip of 80% achievable at 25% H_2 energy share. Also, engine control oriented issues are addressed by demonstrating either intake temperature or diesel fuel share optimization to negate the drawbacks of combustion harshness and NO_X emissions, while improving ITE 1–1.5pp over baseline operation.

Nomenclature

Abbreviations	
BR	Blend ratio
CA50	Crank angle at 50% energy released
CFD	Computational fluid dynamics
CHR	Cumulative heat release
CL	Combustion losses
HCCI	Homogeneous charge compression ignition
HRF	High reactivity fuel
HRR	heat release rate
iEGR	Internal exhaust gas recirculation
IMEP	indicated mean effective pressure
IMEP720	net indicated mean effective pressure
IMO	International maritime organization
ISx	Indicated specific quantity (x: fuel, NO_X, UHC)
ITE	Indicated thermal efficiency
IVC	Intake valve closing
LFO	Light fuel oil
LHV	Lower heating value
LRF	low reactivity fuel
LTC	low temperature combustion
MPRR	Maximum pressure rise rate
MZM	Multizone model
NG	Natural gas
NHR	net heat released
NO_X	Oxides of nitrogen
PCCI	Premixed charge compression ignition
PMEP	pumping mean effective pressure
pp	Percentage points
PRR	pressure rise rate
RCCI	Reactivity controlled compression ignition
RMSE	root mean square error
SE	Standard error
SOC	Start of combustion
SOI	Start of injection
TDC	top dead centre
TDR	Turbulent dissipation rate

(continued on next column)

(continued)

(continued on next page)

This article is part of a special issue entitled: IEEES 2023(Sogut) published in International Journal of Hydrogen Energy.

* Corresponding author.
** Corresponding author.
E-mail addresses: aneesh.vasudev@uwasa.fi (A. Vasudev), maciej.mikulski@uwasa.fi (M. Mikulski).

https://doi.org/10.1016/j.ijhydene.2025.02.152
Received 30 June 2024; Received in revised form 20 January 2025; Accepted 8 February 2025
Available online 18 February 2025

(*continued*)

Abbreviations	
TKE	Turbulent kinetic energy
TKV	Turbulent kinematic viscosity
UHC	Unburnt hydrocarbons
UVATZ	University of Vaasa advanced thermo-kinetic multizone model

Symbols	
°CA	Crank angle degree
$\mathfrak{D}$	Mass diffusion coefficient
k	Turbulent kinetic energy
m	Mass
N_{eng}	Mass
P	pressure
Pr	Prandtl number
Q	heat
R_u	Universal gas constant
Sc	Schmidt number
T	temperature
V	Volume
w	Zone thickness
ε	Turbulent dissipation rate
ζ	Multizone model tuning parameter
ϑ	Kinematic viscosity
λ	Air-fuel equivalence ratio
Λ	Thermal conductivity
ρ	Density

Subscripts	
avg	Average
cyl	Cylinder
i	Species index
iman	Intake manifold
max	Maximum
t	Turbulent
∇	Gradient

1. Introduction

With over $300 billion invested on large-scale projects and production capacity targeted to 38 Mt p.a. by 2030 [1], hydrogen (H_2) is observing a growing demand in the energy domain. This is driven by its utilization in the hard-to-electrify sectors such as in maritime transport, a $1.6 trillion industry [2], where bulk carriers routinely cover over 6000 nautical miles between fuelling stops. These vessels are still powered (≈65% [3]) by fossil based heavy fuel oil, as a result of which the present focus of the industry has been on transitioning to cleaner, low-sulphur options, such as natural gas (NG), marine gas oil (MGO) and methanol. As such, huge potential lies in utilizing H_2, even in admixed form, to reduce carbon intensity but also improve the uptake of this resource.

Among clean combustion concepts, reactivity controlled compression ignition (RCCI) has emerged as a proven technology to simultaneously achieve ultra-low emissions [4] and improved thermal efficiency [5]. It is a dual fuel concept that operates with a low reactivity fuel (LRF) typically premixed with air, and a high reactivity fuel (HRF) is mixed inside the cylinder via (pilot) direct injection. RCCI belongs to the class of advanced technologies called low temperature combustion (LTC) concepts, which enables it to reap the mentioned benefits owing to lower combustion temperatures (T_{max}≈1800K), higher pressure rise rates (PRR), and lean operation [6]. The authors' research group in collaboration with industry partner, Wärtsilä Energy Solutions, has spent several years developing RCCI technology for next-generation marine engines [7,8]. As a result of these efforts, a pilot version of RCCI technology has been moved to sea-trails on board M/V Aurora-Botnia operated by Wasaline. Recently published results [9] of these trials show an order of magnitude lower NO_X emissions (close to automotive Euro VI Level) and methane slip cut down by nearly 50% compared to best-in-class conventional dual-fuel technology.

Still, considerable scope for improvement in this technology exists which withholds it from widespread adoption. These include hydrocarbon emissions at low and part loads [10], combustion stability [11], high PRR [12], and thermal management for efficient after-treatment [13]. In addition, the diverse production pathways that affect the composition of future fuels, combined with the need for flexible fuel operation, position H_2 in an admixed form as a promising solution to address the identified challenges.

Prior investigations on utilizing H_2 in LTC engines, like RCCI and its closely related concept, homogeneous charge compression ignition (HCCI), reveal significant enhancements in engine performance and emission reductions. Hydrogen's high flame speed and wide flammability limits enable mitigation of cyclic variations and combustion instability in both HCCI [14] and RCCI [15] combustion regimes. The addition of H_2 is also used to optimize combustion phasing and duration across various LTC concepts/fuels, including n–heptane fuelled HCCI [14], H_2–ammonia–biodiesel RCCI [16], and H_2–biodiesel RCCI [17].

Under low-load NG-diesel RCCI conditions, H_2 addition has been shown to improve efficiency and engine performance. For instance, Kakoee et al. [18] utilized CFD simulations coupled with the CHEMKIN solver to investigate a natural gas-diesel RCCI engine equipped with a pre-chamber. Their results demonstrated an approximate 5% increase in gross work and indicated fuel conversion efficiency under 30% H_2 addition, albeit with a rise in NO_X emissions due to elevated combustion temperatures. Similarly, Bazrafshan et al. [19] employed AVL FIRE CFD simulations validated against experimental data for a single-cylinder Caterpillar heavy-duty diesel engine. Their study revealed gross indicated efficiencies of up to 64.09% at a gross IMEP of 7.7 bar, 53.53% at a gross IMEP of 6.3 bar, and 53.55% at a gross IMEP of 5.6 bar. Furthermore, cleaner combustion is facilitated by improved combustion efficiency, which manifests itself as a reduction in unburned hydrocarbon (UHC) emissions. For landfill gas-diesel fuelled RCCI [20] a 34% decrease from 0.82 g/kWh in UHC emissions was demonstrated. Similarly, in an experimental study on a single-cylinder RCCI engine, Kalsi and Subramanian found that the fractional addition of H_2 to the NG-biodiesel RCCI mode resulted in a 32% reduction in CO emissions [21].

Despite these benefits, H_2 addition introduces several challenges that necessitate careful management. One significant issue is the increase in combustion temperatures leading to NO_X emissions, as highlighted by Das et al. [22] in H_2-added HCCI diesel engines and by Gharehlar et al. [23] in H_2–diesel RCCI engines, particularly at near-stoichiometric operation and high loads. In the diesel–natural gas dual-fuel RCCI engines, Rahnama et al. [15] conducted a numerical study using CONVERGE CFD to simulate RCCI combustion with H_2 and N_2 blends directly introduced into the intake manifold. Their findings showed that higher H_2 shares significantly increased peak combustion temperatures, resulting in up to a 32% rise in NO_X emissions. Similarly, Ekin et al. [24] used ANSYS Forte CFD simulations validated against experimental data and observed a 12% increase in NOx emissions due to localized temperature spikes from H_2 addition. Another unforeseen issue is a potential increase in UHC emissions [14,25] with excessive H_2 blending, suppressing fresh air aspiration. Similarly, while soot emission is initially reduced, it can increase at higher H_2 percentages due to reduced oxygen availability [15]. The low ignition energy and high reactivity of H_2 pose increased risks of pre-ignition and knocking [26] manifesting as higher rates of pressure rise rate [27] and peak cylinder pressures [28], which increases mechanical stress.

The aforementioned challenges remain areas of active research, posing significant barriers to achieving robust and reliable engine operation with H_2 admixture. Current studies have explored various mitigation strategies. Broadly, these strategies can be categorized into two main groups: injector-related modifications to control combustion phasing, and dilution-based additions to control in-cylinder temperature. The former pertains to methods focused on injection modifications of HRF. Chintala and Subramanian [29] used retarded injection timing to reduce in-cylinder temperatures achieving a 37% NO_X reduction at 18% H_2 share. Duan et al. [30] employed a double DI strategy in

H_2/diesel RCCI to reduce NO_X emissions and improve indicated efficiency. For the second category, direct water injection as explored by Chintala and Subramanian [29] enabled suppression of peak in-cylinder temperature and the heat release rate. Consequently, they reported a 32% NO_X reduction at 18% H_2 energy share, along with an increased maximum H_2 energy share of up to 36% at high engine loads. Rahnama et al. [15] noted that combining H_2 addition with N_2 dilution effectively reduced NO_X emissions without impacting combustion efficiency.

In a similar context, EGR and other diluents have demonstrated significant potential in addressing the challenges associated with H_2 combustion. For instance, Karbasi et al. [31] used EGR to control in-cylinder peak temperatures, achieving EURO VI compliance for NO_X and CO emissions. Karthic et al. [32] found similar results experimentally, reporting that NO_X emissions decreased from 5 g/kWh to 3 g/kWh and 0.9 g/kWh with 5% and 10% cooled EGR. Similarly, Hanafi Gharehlar et al. [23] applied EGR and N_2 dilution to a pure H_2-diesel RCCI engine, achieving thermal NO_X emissions below 0.2 g/kWh, well below EURO VI limits, while improving combustion efficiency to over 51% under low-load conditions. Sattarzadeh et al. [27] employed a combination of injection timing modification and diluents, including EGR (up to 8%) and N_2, to mitigate H_2 combustion challenges in a heavy-duty RCCI engine. The study achieved a H_2 energy share of up to 91%, reduced peak in-cylinder pressures by 36%, and maintained gross indicated efficiencies above 48%, while meeting EURO VI emission standards. Addressing the challenges of H_2 RCCI combustion has seen significant advancements; however, further research is needed to improve the technology's readiness for practical application. A key solution to addressing the primary challenges of H_2 integration lies in maintaining low in-cylinder temperatures, a goal largely achieved through dilution strategies. Another critical factor influencing in-cylinder temperature is intake temperature. While the impact of intake temperature on H_2 HCCI engines is well-documented [33], its effects on H_2-admixed RCCI engines remain underexplored, highlighting a significant research gap in this area.

Thus, summarising the state-of-the-art in literature, H_2 engine studies are widely emerging however focused on light/heavy-duty high-speed engines (<130 mm bore). Application to marine engines differ significantly owing to higher turbocharger efficiency resulting in a positive pressure difference in the cylinder, potentially altering combustion behaviour and performance. Furthermore, research concerning flexible accommodation of H_2 in existing fuel streams, as a feasible way to decarbonise power-demanding applications are in minority, and so far, approached on a fundamental level, with CFD simulations.

Assessing the improvement strategies, in terms of their direct and indirect influence, relative interactions and operating constraints on the system performance calls for an approach more efficient than traditional test cell data-driven calibration or computationally heavy CFD. Model-based development is considered the main enabler to resolve the complexity dilemma. In terms of fidelity, physics-based multizone models (MZM) are positioned in between detailed CFD and empirical models for RCCI combustion simulations. These performance-oriented models are similarly predictive to reactive CFD simulations, while also being computationally light to enable two orders of magnitude faster runtimes. As such, the authors of the present work have developed such a tool – University of Vaasa Advanced thermo-kinetic multizone model (UVATZ), which has been successfully validated on two separate RCCI demonstrators, one [34] based on the Wärtsilä W20DF platform and the other [35] on W31DF. Its utility has been proven towards RCCI control development [36], and system-level engine-aftertreatment calibration [37] and optimization.

The present work is a first mature case study on H_2 admixed RCCI, based on contemporary medium-speed, large-bore engine platform. A first showcase on this topic was presented by Vasudev et al. [38]. at the 14th International Exergy, Energy and Environment Symposium. The current study extends that preliminary investigation with scientific rigor and scope. To this end, the present work employs the latest iteration of UVATZ [34] which is fully autonomous and improves air-fuel mixing and thus, accuracy of emissions prediction. The RCCI experiments conducted on a Wärtsilä's next generation 20DF marine engine, form a basis for simulation-based extrapolation towards flexible incorporation of H_2 into existing fuel streams. This unique methodology, for the first time, allows to bridge the gap between fundamental insights on combustion kinetics of H_2-NG-diesel mixtures, with application-oriented issues of combustion engine control. The established connection forms a milestone towards designing an economically and technologically feasible H_2-based marine propulsion.

The structure of this paper is organized as follows: Section 2 outlines the methodology, detailing the research object, simulation model, and scope of the research. Section 3 presents the results, starting with the baseline model validation in 3.1. The simulation results of H_2 admixed RCCI is comprehensively discussed in 3.2 which includes detailed insights on combustion kinetics. A final subsection, 3.3, discusses measures which allows to optimize engine performance towards higher H_2 energy share under real-world durability and emissions constraint. Drawing from the results, section 4 provides a discussion on practicalities relating to engine operation, hardware changes and optimization for greater performance. Finally, section 5 provides the main takeaways of the paper.

2. Methodology

The description begins with the experimental platform, a state-of-the-art marine engine operating on natural gas and diesel in RCCI mode. This along with measurement dataset forms the basis for model parameterization and validation. A brief description follows, of the predictive, performance-oriented model that will be used in the investigation. Its chemical-kinetics nature enables it to predict H_2 blended performance despite being validated by natural gas and diesel operating conditions. The section concludes with the scope of research for this model-based investigation.

2.1. Experimental reference

In this study, a prototype RCCI research engine based on the Wärtsilä's 20 common-rail dual fuel (CRDF), mid-speed platform is employed. Compared to the commercial variant, everything except the crankshaft and connecting rods are modified for enhanced capability and flexibility for research activities. Housed at Wärtsilä's laboratories in Vaasa, the prototype engine is of the in-line six-cylinders configuration. Table 1 provides a detailed outline of the engine specifications during the experiments. The engine setup includes fully variable electrohydraulic valve actuation for complete control over valve operation and a series-configured two-stage turbocharging system. The fuel system

Table 1
Specifications of the Wärtsilä marine engine used for model identification and validation.

Displacement/nominal speed	8.80 L/1000 rpm
Stroke/Bore	1.4
Air system	Two-stage turbocharged (in series)
High-reactivity fuel system	Common rail
Low-reactivity fuel system	Low-pressure; multi-point, upstream of the intake valve
Valve train	4 valves per cylinder, fully variable hydraulic valve train
Emission system	Horiba Mexa-one (NOX, CO, THC, CO2, O2) AVL415S (FSN-soot)
Indicative system	AVL Indicom, cylinder pressure tranducer Kistler 6124A, 300 bar range, 30 pC/bar sensitivity.
Engine control system	Speed Goat/CanApe rapid control protyping platfrom
Test fuels	LFO compliant to ISO 8217 and NG with MN = 80

incorporates advanced single-needle injectors for direct high-reactivity pilot fuel injection and a multi-point gas injection system upstream of the intake valves. ISO 8217 compliant Light Fuel Oil (LFO), and natural gas with a methane number of 80 are used as pilot and main fuel, respectively. Fuel- and air-path control is governed by a Speedgoat/CANape Rapid prototyping platform using in-house developed Simulink codes.

Data acquisition relevant to this study, includes high frequency measurements of in-cylinder pressure recorded over 300 consecutive cycles with a resolution of 0.2°CA. Consequently, the engine's performance is precisely quantified by further processing the data to calculate apparent heat release, crank angle for X% fuel energy released (CAX), and performance indicators such as indicated mean effective pressure (IMEP). Refer to section 2.3 for details on the post-processing methods involved. To further support accurate model initialisation, the measurement system involves temperature and (fast) pressure measurement in intake and exhaust ports. Low-frequency measurement data further covers liquid fuel consumption, using gravimetric balance and gas (air and NG) mass flow rates using respective Coriolis flow meters. Temperatures of the relevant cylinder components are acquired from thermocouples installed in cylinder head, piston and liner.

Two steady-state operating points from the measurement dataset of the engine are selected (Table 2) as baseline conditions. Cases A and B, are realising RCCI at 20% and 50% engine load, respectively. Both points are with the engine operating at fixed engine speed of 1000 rpm, representative for variable pitch propeller drivetrain or gen-set application. The operating points are characterised by the total air-fuel equivalence ratio (λ) and SOI_{HRF} referring to the injection timing of LFO. Temperature (T) and Pressure (P) with subscript '*iman*' denote the intake manifold thermodynamic state, measured just downstream of the turbocharger. Metering of the two fuels is quantified in relative terms as *LRF/HRF* which defines on mass basis the ratio of NG with respect to LFO. T_{wall} refers to the combustion chamber surface temperature, which includes the liner, head and piston.

From Table 2, worth noting that the operating conditions are characterised by very early LFO injection timing during the compression stroke, to create a nearly premixed, reactivity-stratified conditions typical for LTC. To support proper ignitability of the locally (stratified fuel distribution) and globally (elevated λ) lean mixture, intake temperature in RCCI calibration is elevated compared to conventional dual calibration [4]. Another characteristic feature is that LRF/HRF blend ratio needs to be slightly reduced at low load RCCI operation (Case A) to provide proper distribution of diesel fuel across the whole cylinder volume [40].

Table 2
Experimental operating points.

Case	Load [%]	λ [−]	SOI_{HRF} [°CA bTDC]	T_{iman} [K]	P_{iman} [bar]	*LRF/HRF* (m/m) [−]	T_{wall} [K]
A	21	ref +0.54	ref +36	ref +35.4	ref +0.31	ref −6.25	Liner: 405 Piston: 420 Head: 460
B	50	ref +0.63	ref +31	ref +14.8	ref +1.92	ref +1.09	Liner: 420 Piston: 435 Head: 475

**ref* is the 25% load point conditions on a commercial, conventional dual-fuel version [39] of the experimental engine.

2.2. Simulation model

Fast, performance-oriented simulations are enabled via the in-house developed multizone combustion tool – University of Vaasa Advanced Thermo-kinetic multi-Zone (UVATZ) model. This is a quasi-dimensional model, specifically parameterized for RCCI engine simulations, although it can broadly be used for most LTC concepts [34]. With model development and validation comprehensively expounded upon in our earlier works [34,35], the discussion here is terse to avoid repetition. The important model considerations are highlighted in Table 3. For the convenience of interested readers, all model equations are listed in Appendix 1.

The governing assumption of axisymmetric in-cylinder fluid flow is the basis for discretizing the combustion chamber volume into ring-shaped cylindrical zones (Fig. 1) according to the Lagrangian perspective. Each zone is considered a homogeneous reactor. Furthermore, these zones are assumed to share the same pressure as the bulk combustion chamber pressure. The underpinning for this is the further assumption that pressure difference between the zones equalizes at the speed of sound. As a consequence, the momentum balance equation is not solved. Still, interzonal heat and mass flow is phenomenologically modelled, by considering the gradients of temperature and species concentration, respectively, between neighbouring zones as the driving force. This is analogous to the diffusion process, with the coefficient for diffusion obtained from the sub-model for in-cylinder turbulence [42].

The third assumption is a consequence of the nature of RCCI, wherein combustion is primarily driven by chemical kinetics. Since a large delay occurs between end of fuel injection and the onset of combustion (e.g., 35° – 50°CA observed in the present research) both phenomena can be modelled in a decoupled manner. Thus, the model for LFO injection is simplified, whereby the spray development process is skipped, and the ensuing bulk in-cylinder fuel stratification that triggers combustion, is directly modelled. An empirical model predicts the HRF stratification with respect to operating parameters (injection timing, injected HRF mass and in-cylinder density) and is calibrated on CFD spray simulations. Considering the arrangement of zones (Fig. 1), the fuel stratification is primarily captured in the radial direction of the cylinder. Further background on the approach is presented in our recent work [34], while the model equations are listed in Appendix 1.

Heat exchange with the combustion chamber walls are modelled using the (lumped parameter) heat transfer coefficient, that is computed following the correlation of Chang et al. [43]. This is applied on the zones numbered 10, 11 and 12 (Fig. 1) which correspond to the lumped boundary regions of liner, piston and head. The respective gas side temperatures of these surfaces are in Table 2. The size of all zones as a fraction of the in-cylinder volume is presented in Fig. 2, which has been calibrated based on the predicted heat release profile and emissions

Table 3
Governing assumption of UVATZ model.

Source code	C++ with Cantera libraries [41]
Gov. Assumptions	- axisymmetric in-cylinder fluid flow - common zone pressure - fuel injection decoupled from combustion - Ideal gas
Gov. Equations	Mass, energy & species balance; Eq. Of state (refer Appendix 1)
Zonal configuration	12 zones (10x annular cylider; 2x disc zones)
Interzonal heat & mass flow	Temperature & concentration gradient-based; turbulence energy cascade [42]
HRF stratification	Emperical model trained by CFD spray simulations [34]
Wall heat loss	Chang et al. [43]; zone dependent
Reaction mechanism	Yao et al. [44] + NOx scheme [45]
Validation	Wärtsilä 31DF RCCI [35,46] and 6L20CRDF RCCI [34] full-metal engine
Simulation time	<3min/cycle; desptop PC @Intel Core i5 8th gen
Solver	CVODE [47] tolerance = 1e-9; max. time step = 2e-6s; convergence = 6–8 cycles (1e-3 rel. tol.)

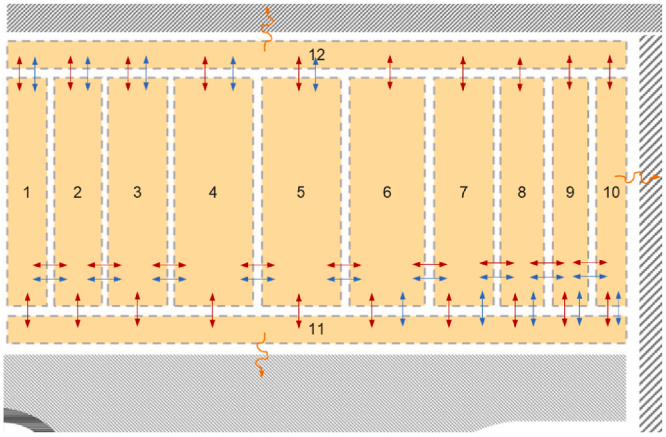

Fig. 1. Schematic of the UVATZ combustion model. Zones are represented by the orange boxes. Red arrows indicate heat flow and blue arrows indicated mass transfer. (For interpretation of the references to colour in this figure legend, the reader is referred to the Web version of this article.)

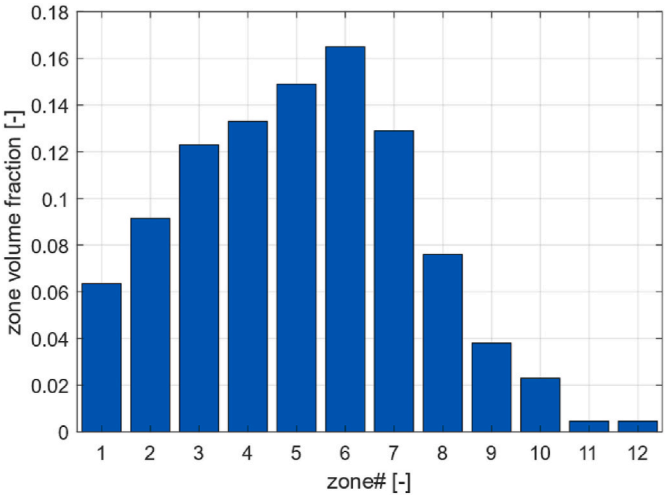

Fig. 2. Zones' size as fraction of total in-cylinder volume. Reproduced from Vasudev et al. [34] with permission from authors.

(NO_X and UHC). These assumptions allow to capture the influence of reactivity stratification, i.e., bulk in-cylinder thermal and fuel inhomogeneity on engine performance, in a computationally efficient manner.

UVATZ simulates only the closed part of the four-stroke cycle. For simulating the full-cycle, therefore, a simple plenum sub-model is supplemented for the gas exchange process. In the approach, the entire cylinder volume is assumed as a single 0-dimensional reactor and is connected to fixed-state objects to represent intake and exhaust plenums. The gas exchange is then modelled as isentropic flow based on imposed valve lift profile between the plenums and cylinder volume. The crucial benefit of this approach is accurate predictions of the initial condition for UVATZ, i.e., thermodynamic state and composition at intake valve closing (IVC), via cycle-to-cycle connected simulations. Ultimately, the simulation time is below 3 min per engine cycle. Consecutive 6–8 cycles are required for convergence, based on relative change in mean effective pressure and P_{max} below 1e-2. The choice regarding chemical kinetics scheme of Yao et al. [44] has been previously validated for NG-LFO RCCI operation in a 310 mm bore [35] and 200 mm bore [34] marine engines.

2.3. Postprocessing methods

The raw output data from the simulation contains the thermodynamic state of each zone including their individual composition histories. Since all zones share a common pressure, the in-cylinder pressure is simply taken as any one of the zone's pressure. The raw pressure data exhibits jagged features which is inherent to such multizone approaches [48]. Hence, a simple moving average filter is applied to smoothen it. The pressure rise rate (*PRR*) is then computed as bar/°CA by applying a Savitzky-Golay filter on the resulting pressure signal, from which the peak value is referred to as PRR_{max}.

Furthermore, heat release rate (HRR) during the cycle is calculated via the apparent heat release approach (Eq. (1)) from the simulated pressure curve. The ratio of specific heats (γ) used here is fixed to 1.368 based on the setup calibration.

$$HRR_{net} = \left(\frac{\gamma}{\gamma-1}\right) P \frac{dV}{d\theta_{CA}} + \left(\frac{1}{\gamma-1}\right) V \frac{dP}{d\theta_{CA}} \tag{1}$$

Additionally, performance indicators that are typically used in assessing engine performance are also postprocessed. First, the quantity, net heat released (NHR) is computed as the integral of HRR over the closed cycle. A cumulative integral on HRR provides the cumulative heat release (CHR) profile. Compared to HRR, it provides a more straightforward visualization of the rate of combustion and the overall fuel energy released during cycle. From CHR, combustion phasing indicator, i.e., CA50, CA10, and burn duration (CA10-90) are determined.

The indicated mean effective pressure (Eq. (2)) is an engine-size independent quantifier of applied load, and is calculated over the full cycle (720°CA) from in-cylinder pressure. Pumping mean effective pressure (*PMEP*) is computed using the same relation, but integrated only over the duration exhaust valve opening (EVO) to IVC. Based on mean effective pressure, the net indicated thermal efficiency (ITE_{net}) is computed as in Eq. (3). The fuel flow rate ($\dot{m}_{LRF}$, $\dot{m}_{HRF}$) of the LRF and HRF combined with their heating value (LHV) gives the available fuel power. V_{disp} is displacement in m^3 and N_{eng} is engine speed in rev/s. Additionally, the pumping loss, i.e., the fraction of fuel energy utilized for powering the open part of the cycle, is also calculated from Eq. (3), but replacing *IMEP* with *PMEP*.

$$IMEP_{net} = \frac{1}{V_{disp}} \oint P\, dV \quad [bar] \tag{2}$$

$$ITE_{net} = \frac{1/2 \cdot IMEP_{net} \cdot V_{disp} \cdot N_{eng}}{\dot{m}_{LRF} LHV_{LRF} + \dot{m}_{HRF} LHV_{HRF}} \text{ x100} \quad [\%] \tag{3}$$

Combustion performance is quantified by the incomplete combustion loss (CL), which is a fraction of fuel energy. In Eq. (4), the energy contained within the emission species of CH4, CO and non-methane hydrocarbon (NMHC) are used. The lower heating value (LHV) of CO is taken as 10.1 J/kg while that for NMHC assumes the same as LFO. Finally, calculation of indicated specific quantities is represented as a generalized expression, Eq. (5), where *x* can be emissions (NO_X or UHC) or fuel consumption. The unit is g/kWh, when the associated mass flow is expressed in g/h and $IMEP_{net}$ as kPa.

$$CL = \frac{\dot{m}_{exh}(Y_{CH4} LHV_{CH4} + Y_{CO} LHV_{CO} + Y_{NMHC} LHV_{HRF})|_{\theta=EVO}}{\dot{m}_{LRF} LHV_{LRF} + \dot{m}_{HRF} LHV_{HRF}} \text{ x100} \quad [\%] \tag{4}$$

$$ISx = \frac{2 \cdot \dot{m}_x}{IMEP_{net} \cdot V_{disp} \cdot N_{eng}} \quad [g/kWh] \tag{5}$$

Note, that the methodology described here is consistently applied to postprocess both simulation and experimental data. This is done to secure model validation results. Refer to section 3.1 for further discussion on model accuracy.

2.4. Scope of research

The scope considers the cross-influences of all three fuels in RCCI combustion, namely H_2, NG, and LFO. Table 4 lists relevant properties of the fuels utilized in this study. Worth noting that the surrogate for NG is a blend of ethane and methane in the ratio 1:24, while LFO is modelled with n-dodecane, as available in the chemical kinetic scheme [44] utilized. Furthermore, since spray process is not modelled, the LFO in vapor phase is considered directly injected into the cylinder while accounting for the evaporation enthalpy in energy balance.

The scope of research encompasses strategies that require minimal hardware changes to the base engine for H_2 fuelled operation. To this end, simulations considers both the low reactivity fuels, NG and H_2, to be port fuel injected (PFI). As such, both are modelled as premixed with air. The only high reactivity fuel, LFO, remains direct injected. Mixing of H_2 in the LRF stream is quantified on energy basis by blend rate (*BR*), defined in Eq. (6). While *LRF/HRF* defined earlier (Section 2.1) parameterizes on mass basis the ratio of overall LRF stream to the HRF.

$$BR = \frac{\dot{m}_{H2}\, LHV_{H2}}{\dot{m}_{H2}\, LHV_{H2} + \dot{m}_{NG}\, LHV_{NG}} \text{ x } 100 \quad [\%] \tag{6}$$

Table 5 presents the simulations categorized into four campaigns, along with indication of the associated boundary conditions. First, validation of the model is conducted on the baseline, NG-LFO fuelled RCCI operation. The operating conditions for cases A and B are the ones mentioned in Table 2, therefore indicated as baseline (BL). Worth bearing in mind that these validation conditions are deemed sufficient for the application of UVATZ to H_2 blended simulations. Owing to the chemical-kinetics basis of UVATZ, the widely validated chemical kinetics scheme [44] utilized, includes the H2/O2 reactions subset which are dominant intermediate species in oxidation of all hydrocarbon and oxygenated fuels. Thus, H_2 combustion is naturally captured by UVATZ. However, the authors acknowledge that despite the possible absolute error in predictions, the predicted trends in performance is of relevance for the scope of this model-based investigation. Furthermore, the predictions following section 3.2 are assessed based on findings from literature which are under similar conditions.

The remaining campaigns deal with H_2 blended operation, thus categorized as 'H_2 admixing' in the table. Campaign two pertains to the study of H_2 blending when the boundary conditions remain unchanged as in cases A and B (Table 2). This is achieved by varying *BR* (in steps of 5%) between 0% and 25%, while the total fuel energy is held at BL conditions. In order to gain further insights on the combustion chemistry, 0-dimensional constant pressure reaction simulations are conducted at engine relevant conditions, explained further in section 3.2.3. Since H_2 influences differently the oxidation of LFO and NG, the conclusions drawn from here are utilized in discussion of the results in section 3.3.

The increased flame speeds and mixture reactivity with H_2 blending has been observed to produce harsher combustion manifested in increased peak cylinder pressure and PRR_{max}. Our previous study [38] showed that combustion harshness could potentially exceed safe design limits especially at higher engine loads. This is in addition to increased NO_X emissions. Two straightforward mitigation measures include reduction of temperature at intake valve closing (T_{IVC}) and decreasing the proportion of the HRF (LFO) injected. This is achieved by lowering the intake manifold temperature (T_{iman}) when increasing *BR*, for campaign 4. While the campaign 5 encompasses increasing the *LRF/HRF* ratio in conjunction with *BR*. Both strategies form an optimization problem with the objective of maintaining the same combustion phasing (*CA50*) as BL, indicated in Table 5. The corresponding results will be discussed in section 3.3. The approach of increasing λ_{total} is excluded since it depends on the capacity of the turbocharger-compressor to deliver higher boost pressure, which increases complexity of the analysis. The strategy of varying SOI_{HRF} is also excluded as it has limited sensitivity on engine performance as compare to the former two approaches. As such, both the studied approaches are in line with the requirement of minimal changes to hardware and operating characteristics of load points (A and B).

Table 4
Properties of the fuels considered in the study.

Properties		H_2	NG	LFO
Density (60°C & 1atm)	kg/m	0.084	0.691	7.08[a]
Viscosity (60°C)	cSt	130.66	20.36	0.829[a]
Specific heats ratio (60°C)	–	1.401	1.281	1.028[a]
Evaporation enthalpy	J/kg	–	–	2.134×10^5
Molar weight	g/mol	2.016	16.6	170.338
LHV	MJ/kg	120	48.42	44.14
Surrogate	–	H_2	CH_4 (96%)	$nC_{12}H_{26}$
From [44]			C_2H_6 (4%)	

[a] vapor phase – LFO surrogate assumed as vapor in the cylinder, with evaporative cooling modelled phenomenologically in UVATZ.

3. Results and discussion

3.1. Baseline model validation

The simulations by UVATZ are validated against baseline condition of NG and LFO fuelled RCCI operation (Table 2). The validation criterion is based on reproducibility of the high frequency measurement data of in-cylinder pressure and engine performance indicators derived from it. Convergence of the simulations is achieved after 8 cycles, and the results presented below pertain only to the last cycle. Fig. 3 presents the comparison of experimental and predicted in-cylinder pressure and heat release rate for both cases. The pressure curve is normalized to the peak value (P_{max}) from measurements. The cumulative heat release (CHR) profile is normalized to total fuel energy of case of the respective cases.

The simulated pressure curve closely aligns with experimental signal, quantified by an RMS error of less than 1 bar for Case A and 1.56 bar for Case B. The accuracy of P_{max} is within an average of 3% error, while a slight overestimation in the position of peak pressure (P_{max} pos.) by at most 3°CA. The CHR trace of the simulation corresponds well with the experimental trace, with an RMS error around 740J. Furthermore, the occurrence of 50% fuel energy released, noted as *CA50*, is within 1.5°CA absolute error. Worth noting the jagged features in pressure trace that was just mentioned, is especially apparent in the CHR plot. This is due to the sequential autoignition of zones, seen by the pattern of short delay and rapid energy release.

Overall accuracy in predictions by UVATZ is captured among various engine performance indicators as shown in the top plot of Fig. 4. The 5% limit is target accuracy within which the model must perform. The parameters for combustion phasing, *CA10* and *CA50* are predicted with a relative error of −0.52% and +0.48% respectively. In absolute terms, this corresponds to about 1.5°CA, which is remarkable for a predictive model. From the earlier discussion of pressure curve, P_{max} pos. is overestimated by 0.8% on average. P_{max} on the other hand is underestimated by an average of 1.9%. The pressure rise rate which is computed as the first derivative on the basis of °CA. As such, its peak value (PRR_{max}), is typically challenging for multizone models to predict well. However, the applied moving average filter has aided in its prediction to lie within 5% error target.

The net heat release (*NHR*), which is the CHR at the end of combustion, has a large overprediction (4%) for case A as opposed to the mid-load case. This is attributed to inaccuracies in the measured fuel flow rate that has been imposed as boundary conditions. This error has a knock-on effect on $IMEP_{720}$ which is also overpredicted. Despite P_{max} being underpredicted for case A, the inaccuracy in fueling manifests in the overestimated pressure trace during the expansion stoke (Fig. 3).

The bottom plot of Fig. 4 assesses emissions prediction. The accuracy target here is relaxed to 35%. This is due to the generally well-known challenge in accurately predicting emissions. The ultra-low levels of NO_X make it very sensitive to temperature, while unburnt hydrocarbon

Table 5
Simulation conditions for validation and H2 blending investigation. BL refers to the corresponding baseline operating conditions mentioned in Table 2.

Study			Campaign #	Test fuels	Test case	T_{iman} [K]	LRF/HRF [−]	BR [%]
Validation			1	LFO (DI) NG (PFI)	Case A Case B	BL	BL	0
H_2 admixing	*a)* Effects		2	LFO (DI) NG (PFI)	Case A	BL	BL	0 ↔ 25% FE=BL
				H_2 (PFI)	Case B	BL	BL	0 ↔ 25% FE=BL
	b) Optimization	*i)* T_{IVC}	3		Case B	(BL-15) ↔ (BL+15) CA50 = BL	BL	0 ↔ 25% FE=BL
		ii) LRF/HRF	4		Case B	BL	BL ↔ (BL + 15) CA50 = BL	0 ↔ 25% FE=BL

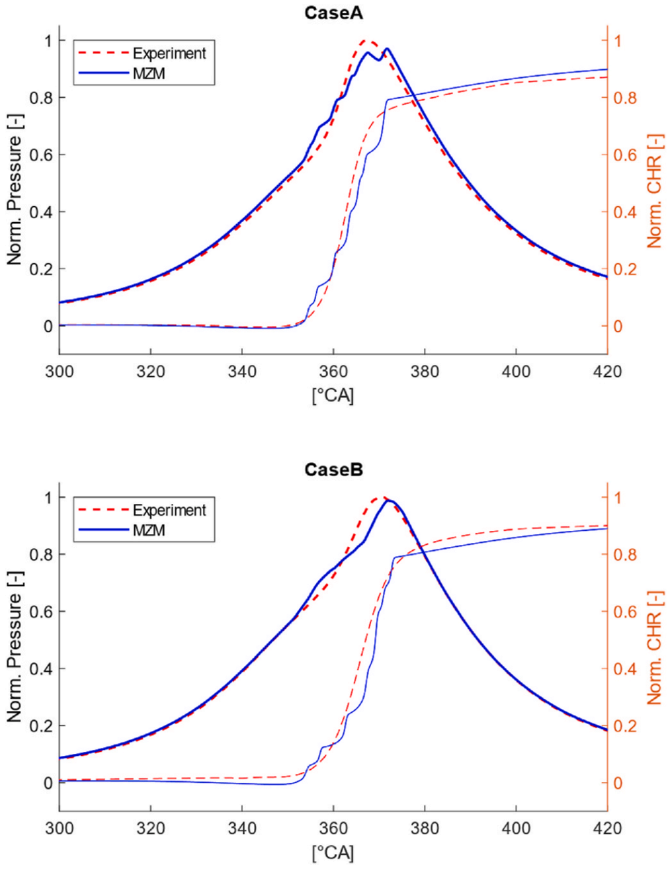

Fig. 3. Comparing simulated and experimental in-cylinder pressure on the left axis and net CHR on the right axis, for case A (top) and case B (bottom). Pressure trace is normalized to peak measured data. CHR is normalized to total fuel energy.

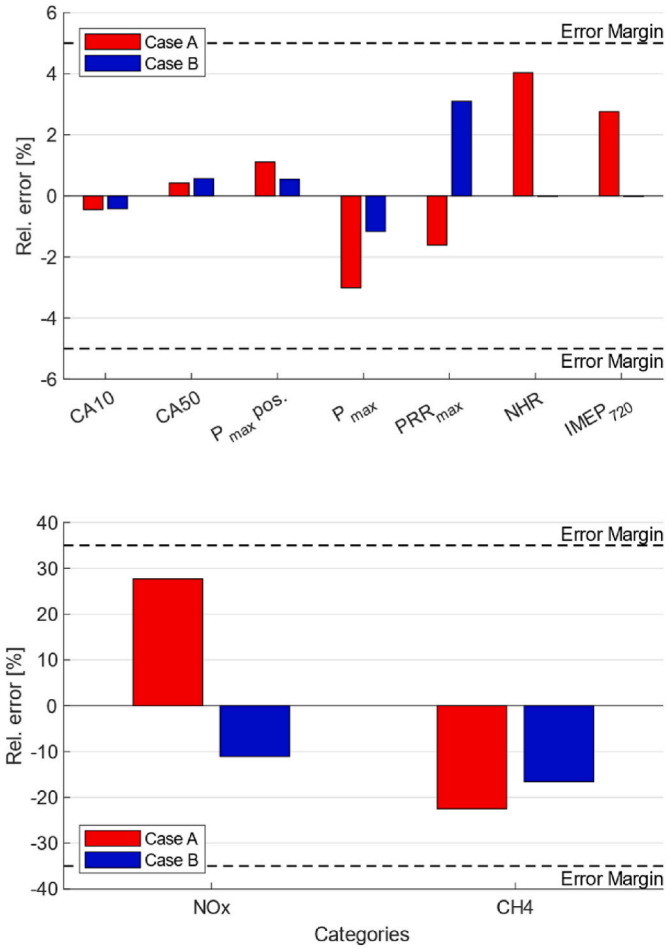

Fig. 4. Relative error in predictions by UVATZ of the synthetic performance parameters (top) and emissions of NO_X and CH_4 species (bottom).

emissions, specifically CH_4 here, depends on how well the boundary zones are resolved and requires accurately prescribed wall temperatures. The reason for choosing 35% as target is that no other MZM in literature except a recent study [49] has approached it. Our recent work [34] in establishing a state-of-the-art autonomous MZM, has comfortably achieved this target. Presently, the results indicate that NO_X is predicted with an error of +27% for case A and −11% for case B. CH_4 emission on the other hand, is underestimated in both cases by 22.50% and 16.59% respectively for A and B.

The validation results demonstrate that especially with respect to engine performance parameters, the model is capable of qualitative representation of H_2 blended operation. The model's accuracy, on the other hand, serves as a basis for determining the statistical relevance in quantitatively assessing the predictions. Critical evaluation from this perspective will be included in the results discussion that follows.

3.2. *Effects of H_2 admixing*

3.2.1. *Combustion analysis*

Considering fixed plenum temperature and λ_{total} (fuelling and boost pressure) the results of varying H_2 energy share in the LRF stream (indicated by *BR*) on RCCI performance are discussed. Detailed plots of crank angle resolved quantities are illustrated only for case B simulations (Figs. 5 and 6) in the interest of brevity. Fig. 5 depicts the directly measurable signal of in-cylinder pressure for the *BR* sweep. The curve, $BR = 0\%$, represents baseline operation, i.e., without H_2 blending. It can be observed that peak value of pressure increases with *BR*, in addition to

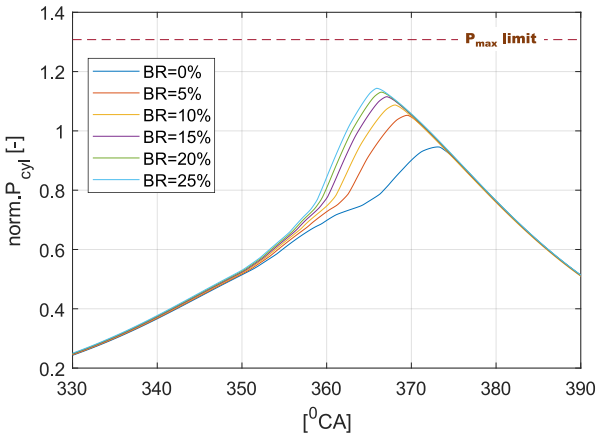

Fig. 5. In-cylinder pressure for BR sweep based on case B operating conditions. Data is normalized to peak value of pressure of baseline case B.

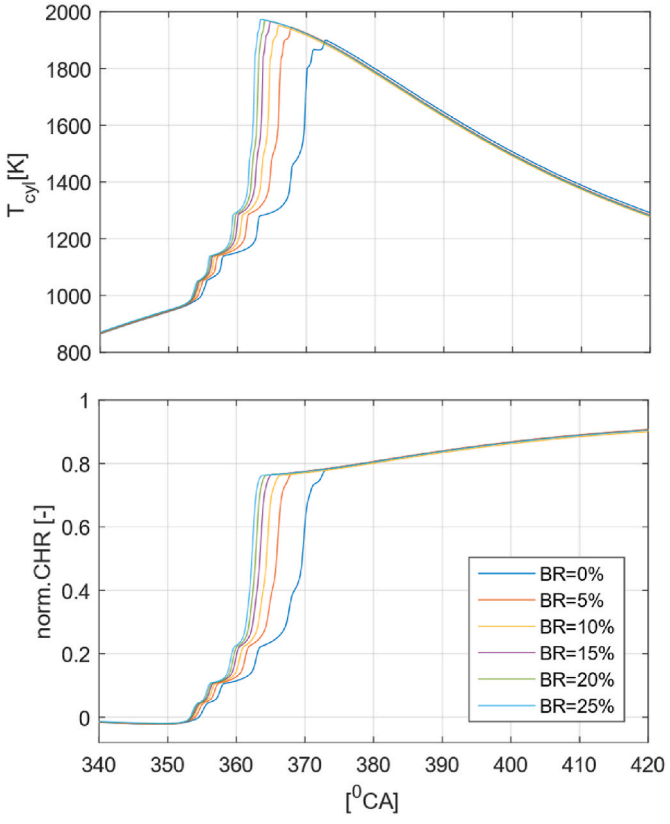

Fig. 6. In-cylinder temperature (top) and net CHR normalized to total fuel energy (bottom) for BR sweep, with case B as baseline operation.

its position shifting earlier. The peak pressure initially increases at a rate of 3.8 bar per percentage point (pp) increase in *BR*, and eventually saturates to around 0.5 bar/%H_2 when *BR*>20%.

In Fig. 5 the occurrence of P_{max} correspondingly shifts to the left initially at a rate of 0.7°CA/%H_2, which then saturates to 0.1°CA/%H_2. This trend is justified by similar observations on position of P_{max} in Kalsi et al. [21] and Rahnama et al. [15]. The reason is due to advancing combustion phasing, supplemented by increasing rate of combustion propagation. Throughout the *BR* sweep, the pressure curve remains within the design limit for P_{max} indicated by the dashed line. It can hence be inferred that the P_{max} is not a limiting factor for blending up to 25%.

The postprocessed CHR including bulk in-cylinder temperature are illustrated in Fig. 6. Compared to baseline operation (*BR* = *0%*), H_2 invigorates the combustion rate observed by the steeper rise in temperature and heat release. The peak temperature increases beyond 1900K already at 5% *BR*. The CHR profile exhibits the trend of shifting to the left, indicating advancing ignition; in addition to the steeper gradient, indicating faster combustion propagation. This is in line with observations [50] for the influence of hydrogen on high octane fuels like NG, which causes a reduction in the ignition delay, as will be elaborated in section 3.2.3.

As in Fig. 5, a non-liner trend is also observed in peak temperature (T_{max}). The initial increase in T_{max} i.e., between *BR* of 0% and 5%, is 43K which then saturates to within 3.5K between 20% and 25% *BR*. Similarly, the occurrence of T_{max} changes initially at the rate of 1°CA/%H_2, which eventually reduces to 0.2°CA/%H_2. These trends are line with the results of [24]. The reason is attributed to hydrogen's influence in accelerating chain branching reactions due to increased presence of radicals such as OH and HO_2, explained further in section 3.2.3. Although the ratio of specific heats (γ) of H_2 is higher than that of CH_4 (Table 4) its influence is relatively minor [50,51].

Trends in combustion phasing (*CA50*) and burn duration (*CA10-90*) are shown in Fig. 7. The data is presented for both cases (A and B), as absolute difference with respect to the results of case A at *BR* = 0%. *CA50* displays a decreasing trend, similar to observations in the works [15,28]. In Fig. 7 the average rate of fall is 0.3°CA/%H_2 considering both cases. This follows from the trend in CHR where the curve shifts to the left, indicating advancing combustion phasing. The reason is mainly due to the shortening of the duration *CA10-50* which happens at a similar rate as the advance of *CA50*.

It is important to note that while advancing CA50 does improve performance, as in case B, its effect also reverses when the curve crosses firing TDC. This happens in case A, where CA50 begins to occur before TDC for *BR*>10%. Inference on engine performance can be made from *CA10-90* where the increasing trend case A reveals that burn duration is extended. The gradient of 0.45°CA/%H_2 is quite steep, compared to that for case B where it is relatively flat. Thus, the prolonging *CA10-90* is an indicator of poor combustion performance, and will be explained in the following section.

3.2.2. *Performance and emission indicators*

Further insights on combustion performance can be obtained from

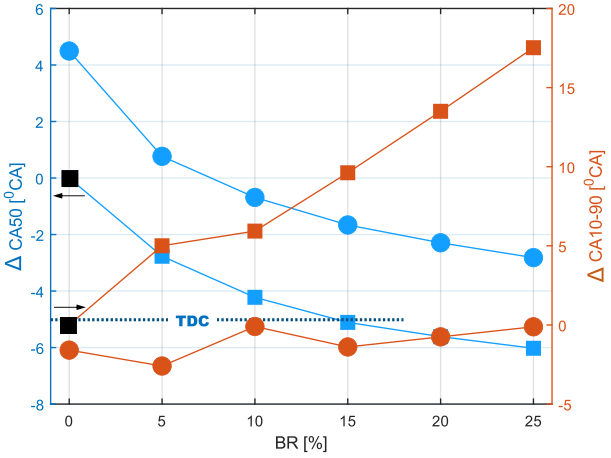

Fig. 7. Variation of CA50 (blue) and CA10-90 (red) with BR, for case A(■) and case B(●). Data is presented as absolute difference with reference to baseline case A results (black ■) of CA50 and CA10-90 on the respective axes. Dotted line indicates firing TDC. (For interpretation of the references to colour in this figure legend, the reader is referred to the Web version of this article.)

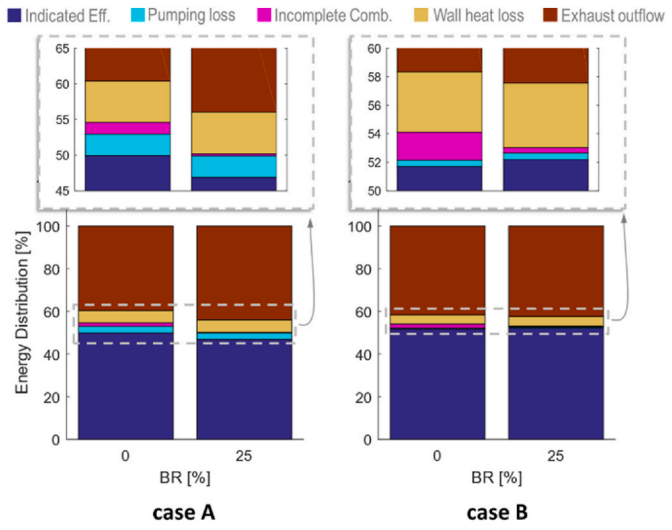

Fig. 8. Sankey chart of the different consumers of total fuel energy, shown with respect to BR of 0% and 25%. The dashed boundary represents the zoomed region shown above, for the respective cases A and B.

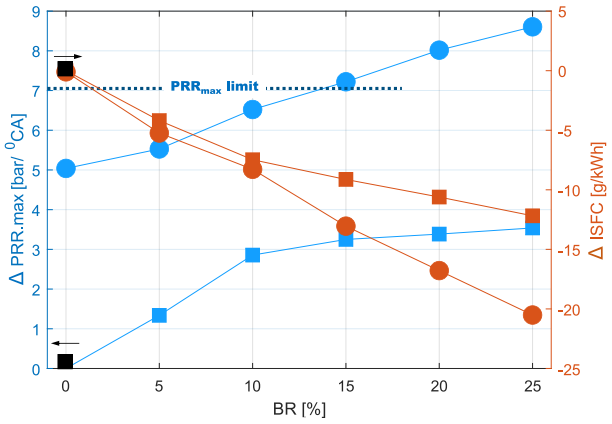

Fig. 9. Variation of PRR_{max} (blue) and ISFC (red) with BR, for case A(■) and case B(●). Data is presented as absolute difference with reference to baseline case A results (black■) of PRRmax and ISFC on their respective axes. Dotted line indicates the PRR_{max} limit of the engine. (For interpretation of the references to colour in this figure legend, the reader is referred to the Web version of this article.)

the Sankey chart (Fig. 8). The bars represent the various consumers of the total available fuel energy. In order not to visually overburden the reader, the data is shown only for *BR* of 0% and 25%, since a monotonic trend is exhibited in the displayed quantities. The data indicates that the proportion of incomplete combustion reduces with *BR*. Specifically at *BR* of 25%, combustion efficiency improves by 1.4% (percentage difference) from 98.34% (BL value) for case A, and for case B by 1.57% from 98%. There are two contributing factors for this trend. First, the increasing combustion temperature results in more complete combustion. Second, the reducing share of hydrocarbon fuel with *BR*.

The increasing combustion efficiency translates to improves indicated thermal efficiency as observed for case B. The efficiency improves by 0.48% (at 25% *BR*) over the already excellent BL value of 51.7%. The backdrop for this is that pumping losses remains nearly constant at 0.44% throughout the *BR* sweep. Heat loss (to environment) shows a minor increase of 0.2% owing to increasing temperature, while the average is around 4.4%. On the other hand, energy lost to exhaust flow increases by 0.7% from 41.65% at *BR* = 0%, owing to the higher enthalpy.

Despite improved combustion efficiency, the trend in case A for indicated efficiency shows a decrease from BL operation. This observation neatly fits into the inference from Fig. 7, where poor combustion phasing was observed at high *BR*. Specifically, for BR>15%, *CA50* occurred before TDC accompanied by prolonging *CA10-90*. This is despite pumping losses (2.9%) remaining flat throughout the *BR* sweep, as well as heat loss, where the value is 5.8%. Thus, unoptimized *CA50* is the fundamental reason for the degrade in case A performance.

Indicated fuel consumption (*ISFC*) as defined in Eq. (5) is shown in Fig. 9. The data is presented as absolute difference with respect to *BR* = 0%. The straightforward explanation is that on mass basis, H_2 has nearly 2.5 times more energy content as NG or LFO (Table 4). ISFC decreases at the rate of 0.5g/kWh/%H_2 for case A and 0.8g/kWh/%H_2 for case B. The decrease in case A is smaller, following the explanation of Figs. 7 and 8, where performance degraded due to poor combustion phasing. IMEP was excluded from the plots since it showed little sensitivity (0.01 bar/% H_2) to BR.

The implication of H_2 blending is also the risk of crossing the durability limits of the engine components. One of the indicators, P_{max}, already showed (Fig. 5) that despite increasing with H_2 energy share, it remained well within the limit of 250 bar of the engine. Another measure is peak pressure rise rate (PRR_{max}) shown in Fig. 9. The observed trend is similar to the work [24]. For increasing H_2 energy share, PRR_{max} for case A is within durability limits of 10 bar/°CA. However, for case B operation, the limit is exceeded around *BR* of 13%. Already for *BR* of 10%, the operation is just 0.4 bar/°CA under the PRR_{max} limit. Thus, combustion harshness, characterized by excess noise and vibrations, becomes a limiting factor for H_2 blending for mid-to high-load operating conditions. This can be typically addressed by optimizing combustion phasing, as will be discussed in section 3.3.

The main emissions of concern are that of particulate matter (PM), UHC and NO_X, specifically the species, NO and NO_2 for the latter, as regulated for instance by European commission [52]. With RCCI operation producing little to no smoke, PM emissions are of no concern. Furthermore, with over 80% of the fuel energy share from NG (Table 2),

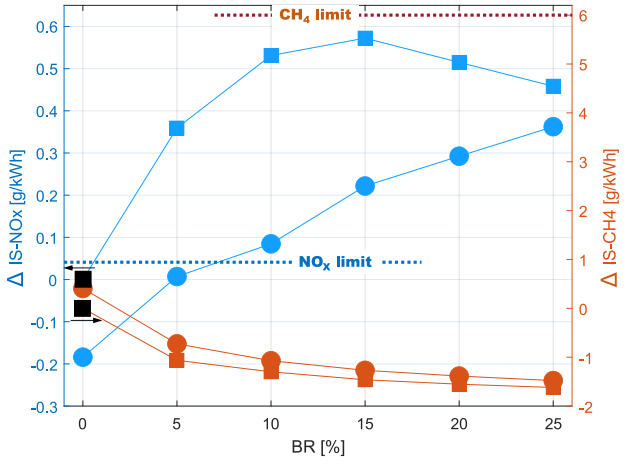

Fig. 10. Variation of indicated specific NOX (blue) and CH4 (red) emissions with BR, for case A(■) and case B(●). Data is presented as absolute difference with reference to baseline case A results (black■) of IS-NO_X and IS-CH_4 on their respective axes. The dotted lines indicate the emissions limit according to EU stage V inland waterways legislation [52]. (For interpretation of the references to colour in this figure legend, the reader is referred to the Web version of this article.)

UHC majorly pertains to CH_4 emissions. These emission species are shown on indicated specific basis in Fig. 10, where the trends are line with other works [15,31] from literature. Also annotated are the strict emissions limit for NO_X and CH_4 as stipulated according to EU stage V inland waterways regulation [52]. The limit for NO_X for the current engine category is 0.4g/kWh and for CH_4 is around 8.3g/kWh. Note that a conversion factor is applied on the brake specific limits in order to make them consistent with the indicated specific basis shown in the plot.

It can be observed from Fig. 10 that at BL calibration ($BR = 0\%$) for both cases, NO_X and CH_4 emissions are already below the regulation limit. Worth mentioning here that in making the comparison with respect to the regulation limit, accuracy of emissions prediction by UVATZ needs to borne in mind. Taking the example of NO_X, difference between the prediction and regulation limit value is 10 percentage points, which is smaller than the emissions accuracy of 30% (Fig. 4). As such, caution needs to be exercised. However, the trends are correct, as mentioned earlier (section 1) and allows for meaningful conclusions to be drawn.

Low levels of NO_X measured at the cylinder exhaust port is a consequence of the low-temperature nature of RCCI combustion. Remarkably, CH_4 emissions is well below the EU stage V regulations by nearly 75%. Worth mentioning that this substantiates the claim that the present research basis itself on real-world, calibrated load points on-board (Table 2) marine engines.

NO_X emissions increase with H_2 energy share and is a result of increasing in-cylinder temperature (Fig. 6). Worth noting that the reaction scheme used for NO_X in UVATZ only considers the thermal formation route. The average rate of increase of NO_X with *BR* is approximately 0.02g/kWh/%H_2 for case B. However, for case A, an inflection point can be observed at *BR* of 15%, after which NO_X reduces. The explanation lies in the observation made earlier on CA50 (Fig. 7), which begins to occur before TDC, and results in an overall drop in engine performance (Fig. 8). Importantly, at *BR* of 1% and 7%, for cases A and B respectively, the NO_X limit is exceeded. This may not be a limiting factor to operate the engine with H_2 blending, since after-treatment devices (SCR) can be used as a mitigation measure.

The CH_4 emissions, on the other hand, displays a decreasing trend for both cases. This corresponds well with Fig. 8, which demonstrated a decrease in unburnt fuel power with BR. As such, this trend is a result two contributing factors, namely, increasing combustion temperature and reducing hydrocarbon fuel share. The CH_4 emission thus drops below the baseline operation of both cases, and well below the stage V emission standard by nearly 90%.

Finally, CO_2 emissions are reduced (Fig. 11) due to increasing energy share of H_2. As such, CO_2 on indicated specific basis, reduces at a rate of 2.8g/kWh/%H_2 for case A, and 3.5g/kWh/%H_2 for case B. Compared to baseline operation ($BR = 0\%$), a reduction by 21% in CO_2 emissions can be achieved at a *BR* of 25%. Furthermore, an overall perspective of all emission species examined, can be obtained from an effective GHG emission. Specifically, CO_2, CH_4 and N_2O can be processed to determine the gram equivalent CO_2 emissions. The calculations use global warming potential (GWP) of the respective species following the intergovernmental panel on climate change (IPCC) standard [53]. A decreasing trend is observed with an average rate of 5g/kWh/%H_2. This is despite the increase in NO_X, since it is smaller in magnitude with respect to CH_4 and CO_2, and the fact that N_2O contributes to less than 5% in NO_X composition. As such, this conclusively substantiates the benefit of H_2 admixing from a take-to-wake basis.

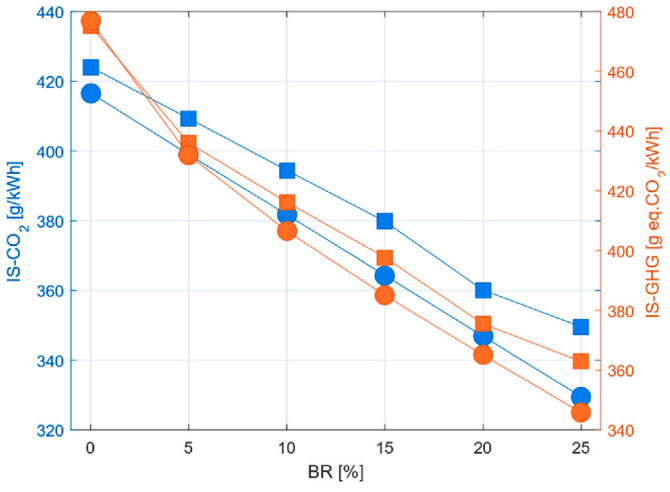

Fig. 11. Indicated specific emissions of CO_2 (blue) and effective GHG emissions (red) as g equivalent CO_2, for case A(■) and case B(●). Effective GHG includes CO_2, CH_4 and N_2O and uses respective GWP values from [53]. (For interpretation of the references to colour in this figure legend, the reader is referred to the Web version of this article.)

3.2.3. *Insights from combustion kinetics*

With autoignition being a driving mechanism for RCCI combustion, the influence of the three interacting fuels on the combustion behaviour results observed above, is further discussed. H_2 admixture has opposing effects on high reactivity fuels like $C_{12}H_{26}$, as opposed to low reactivity fuels like CH_4. Reyhanian and Hosseini [51] note that H_2 results in an increase in autoignition time when admixed with C_7H_{16}, caused by suppression of low temperature heat release, and the main, high temperature heat release, delayed. On the other hand, for CH_4 they note that H_2 blending causes a decrease in autoignition time, with increased vigour in combustion rate. These observations are also in line with Guo and Neill [14] and Voshtani et al. [50].

As mentioned, this behaviour is related to the reactivity differences between the three fuels. In order to illustrate this, simple ignition delay simulations are performed for constant pressure combustion processes. In order to reflect engine relevant conditions, the initial temperature and pressure are set to 1000K and 140 bar respectively. This condition approximates the duration between *CA10* and *CA50* observed in section 3.2.1. The composition for fuels follows the same *LRF/HRF* as in cases A and B, with λ_{total} fixed to 2. *BR* of 0% reflects that the fuel mixture is exclusively NG and LFO, while *BR* of 100% indicates LRF is composed solely of H_2.

A simple definition for ignition delay is employed, defined as the time required for the temperature in the reactor to rise by 200K. The results are documented in Table 6, showing that the autoignition time for H_2 with $C_{12}H_{26}$ is nearly half that of CH_4 with $C_{12}H_{26}$, for both cases. Furthermore, ignition delay times for case A is shorter than those for case B. This is due to a larger fraction of HRF in case A than in Case B. Ultimately, it can be inferred that reactivity of H_2 is greater than that of CH_4, and less than $C_{12}H_{26}$.

Table 6
Ignition delay time for constant pressure combustion simulations with initial T and P of 1000K and 140 bar respectively.

BR [%]	Ignition delay [ms]	
	LRF/HRF	
	case A	case B
0%	1.05	1.58
100%	0.58	0.84

This explains the reason why combustion phasing advances with H_2 admixing for cases A and B. This is due to the larger fraction of CH_4 compare to $C_{12}H_{26}$ in both cases, which dominates the overall combustion behaviour. As such, insight on the reactions that influence the main phase of CH_4 oxidation can be obtained by a sensitivity analysis. This is conducted via constant pressure combustion simulation as above. The initial temperature and pressure are set to 1000K and 140 bar, respectively, reflecting the conditions between CA10 and CA50 for case B operation. The fuel mixture (*LRF/HRF*) follows from case B. The sensitivity calculated here is that of CH_4 concentration with respect to the reaction rate constant of all the reactions within the H_2/O_2 and CH_4 oxidation scheme of [44]. Thus, a normalized sensitivity coefficient (S_i) is computed [41] as in Eq. (7), with subscript *i* referring to the associated reactions.

$$S_i = \frac{k_i}{Y_{CH4}} \frac{\partial Y_{CH4}}{\partial k_i} \tag{7}$$

The results in Fig. 12 gather some of the most influential reactions on CH_4 consumption, for *BR* of 0%, i.e., no H_2 blending, and *BR* of 20%. The negative values of sensitivity coefficient indicate consumption or reduction in CH_4 concentration. Under H_2 admixture, the hydrogen peroxide (H_2O_2) recombination/dissociation reaction (R18) is influential [54]. This is a pressure dependent reaction, bearing its influence at the intermediate temperatures and high-pressure region. It is connected to R14 in the consumption and production of HO_2 active species. R1 is the most important chain branching reaction [55] of H_2 oxidation with production of hydroxyl radical (OH), which is critical for accelerated combustion of H_2 and CH_4. Likewise, R3 also proves critical at intermediate temperature (<2000K) for rapid reaction rates. Interestingly, R73 shows high sensitivity for the simulation without H_2 blending, since methyl radical (CH_3) is the main driver of CH_4 oxidation [56] after combustion has initiated (CA10). On the other hand, R89 is a critical mode of CH_4 consumption based on OH radicals from the H_2 blending. As such, with H_2 admixed, CH_4 combustion is driven.

3.3. Combustion optimization

The results discussed in section 3.2 showed that at higher energy shares of H_2, firstly results in harsher combustion, quantified by PRR_{max} exceeding the engine durability limits, particularly at elevated engine loads. Secondly, NO_X emissions simultaneously increase, potentially crossing the regulation limits. Third, the advancing *CA50*, especially near TDC and crossing it, reduces the ITE, IMEP and increases losses.

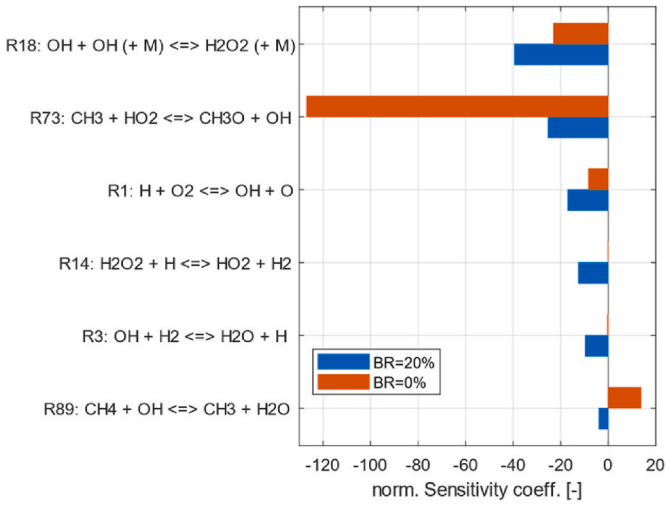

Fig. 12. Sensitivity analysis of CH_4 concentration (mass fraction) with respect to reaction rate constant of H_2/O_2 and CH_4 elementary oxidation reactions within [44], at different H_2 blends.

Thus, despite the inherent benefits of H_2, poor performance is observed due to unoptimized engine control parameters. This section independently explores T_{iman} and *LRF/HRF* ratio, as single factor optimization. These control parameters are chosen as both are in line with minimal hardware changes for retrofitting existing engines, while also having large influence on performance. The objective is to achieve the same *CA50* as baseline results, as this was already optimized calibration from the RCC engine (Table 2). The constraints include the PRR_{max} and EU stage V NO_X limits.

3.3.1. Intake temperature control

Temperature at IVC has huge influence on reaction rates and as such is one of the most effective measures for RCCI control [13]. In the engine considered here, fast temperature control is facilitated by variable valve actuation. Range of this control can be further increased by employing a slower intake temperature control facilitated by intercooler bypass. To reflect the net effect in the simulation, the intake valve closing temperature (T_{IVC}) is varied, by correspondingly changing the T_{iman}. As such, for each level of *BR*, T_{IVC} is optimized with the objective to match *CA50* to baseline operation.

The results compiled in Fig. 13 correspond to case B since both the PRR_{max} and NO_X limits were exceeded. Worth noting that due to the low reactivity of NG, already at baseline operation for case B, the T_{IVC} is nearly 100K above ambient, at a boost pressure around 4 bar. The top plot of Fig. 13 shows that T_{IVC} must be reduced with increasing H_2 energy share, to keep CA50 at baseline level. The consequence of this on

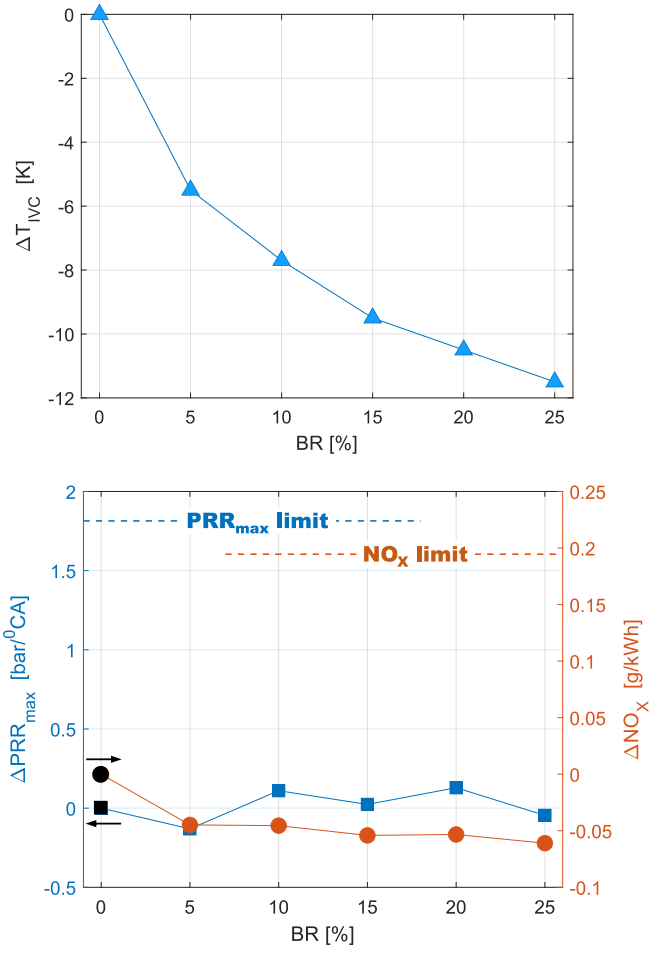

Fig. 13. top – controlling T_{IVC} with BR to match baseline CA50; bottom – the resulting PRR_{max} and NO_X emission. Data is presented as absolute difference with respect to baseline case B condition (black).

engine performance is shown in the bottom plot. While earlier (Fig. 9) the PRR_{max} crossed the engine's durability limit at *BR* of 15%, now is around the baseline value. Although not shown, P_{max} correspondingly showed a similar trend, of hovering about the baseline value. Similarly, while NO_x emissions showed an increasing trend earlier (Fig. 10) of crossing EU stage V limit at *BR* 10%, now slightly falls from baseline value.

The reason is that initial temperature influences the overall reactivity of the mixture, thus decreasing T_{IVC}, reduces mixture reactivity. The sensitivity of NO_X to T_{IVC} is 0.021g/kWh/K when no H2 is admixed, and this increases with blending, for instance, at $BR = 15\%$, the gradient is 0.035g/kWh/K. However, such a strategy did not negatively impact engine performance, with ITE at all *BR* levels matching baseline operation.

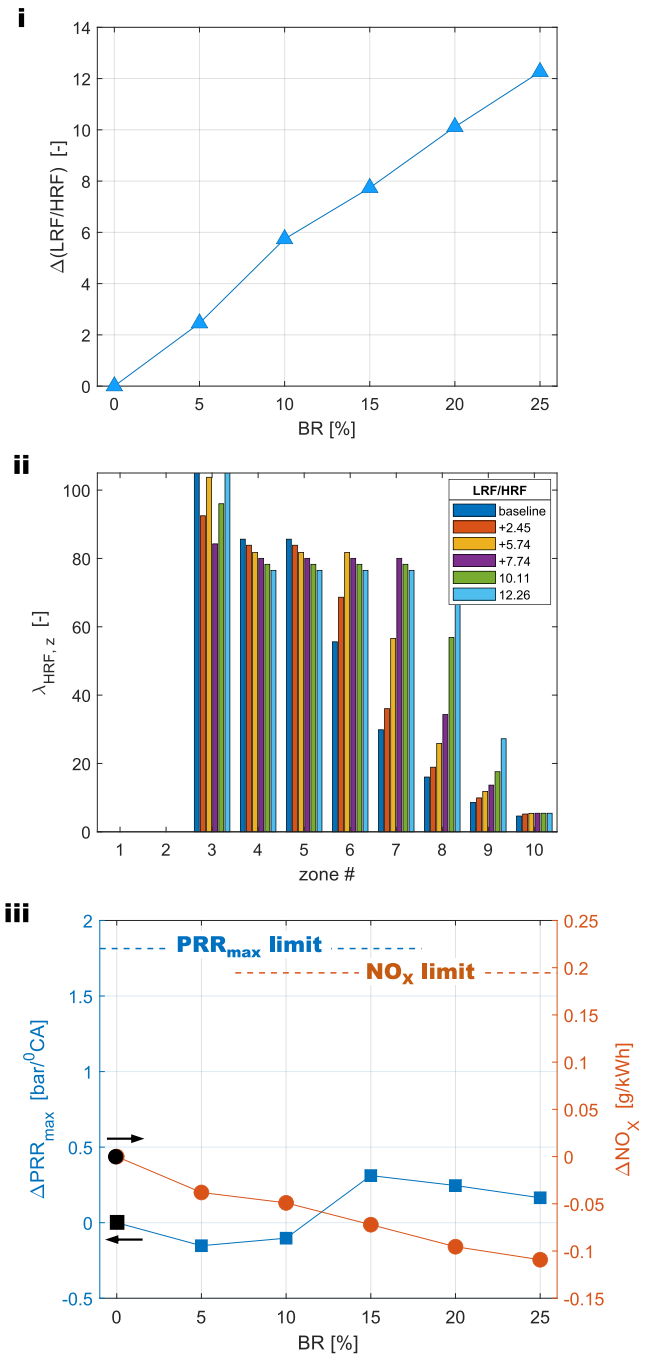

Fig. 14. For case B i) controlling LRF/HRF with BR to match baseline CA50; ii) resulting change in HRF stratification in the zones ($\lambda_{HRF,z}$) of UVATZ; iii) influence on PRR_{max} and NO_X emission, where data is presented as absolute difference with respect to baseline condition (black).

3.3.2. *Fuelling control of LRF/HRF*

The second strategy is related to changing the proportion between the HRF (LFO) and LRF, i.e., *LRF/HRF* ratio. This is achieved by controlling the individual fuelling of LFO, NG and H_2, while still maintaining the same total fuel energy input as baseline. Additionally, the manifold conditions of temperature and λ_{total} are also fixed. The simulations are carried out by accordingly changing the fuel flow rates resulting in a change in *LRF/HRF*.

The results are compiled in Fig. 14, with the top plot showing the variation of *LRF/HRF* for each *BR*. An increasing trend is observed, indicating the share of LRF is raised. In other words, overall reactivity of the fuel mixture is decreases, due to decreasing share of HRF. As such, this strategy is similar to the previous, in that mixture reactivity is decreased with increasing H_2 energy share. A consequence of reducing the quantity of injected LFO, is on the resulting HRF stratification. This is captured by UVATZ, and the results are shown in Fig. 14ii, as the local equivalence ratio of HRF in each zone ($\lambda_{HRF,z}$). It can be observed that the concentration of HRF in each zone decreases. This mimics the radial profile of HRF concentration observed in reality [57], in the form of zone-wise distribution.

Fig. 14iii shows the influence of this strategy on engine performance. By modulating mixture reactivity, the engine operates with similar harshness as the baseline, within the engine's PRR_{max} barrier. Regarding NO_X emissions as before, there is further potential for reduction. Although not shown, CH_4 emissions is maintained at baseline, thus operating with both emission indicators below EU stage V standard. Regarding combustion characteristics, worth noting that as *CA50* is maintained at baseline, burn duration also followed suite. The rate of increase of ITE is observed to be very small, with best value of 1.2 pp above baseline achieved at $BR = 25\%$. However, in this regard, it is worth exercising causing, as the predicted increase is at the cusp of statistical relevance by the model.

While both strategies can be employed for similar efficacies of reducing combustion harshness and emissions, there are certain practical considerations that differentiate their benefits from each other. The first is number of control parameters and therefore, the complexity of the controller. Additionally, the former strategy can be viewed from the perspective of reduction in intake air preheating. This is typically necessary at low and part load conditions due to reduced reactivity. Another point of view of assessment pertains to CO_2 reduction. Owing to the reducing fractions of HRF in the second strategy, for $BR = 25\%$, the CO_2 can be further reduced by 5% compared to the first strategy.

4. Study limitations and outlook for further work

The methodology used thus far mainly focused on single parametric sweeps. And the conclusions are drawn that key performance indicators such as *IMEP* and *ITE* do not drop below baseline with H_2 admixing. As such, no particular attention was directed towards maximizing *ITE*. However, our previous study [38], which was conducted on a different engine (higher compression ratio than the present), showed that 1–2% difference improvement in ITE can be achieved. Hence, there lies unexplored potential in multiparameter optimization of the engine towards higher operating efficiency.

The initial sweeps on *BR* (Fig. 7) demonstrates the influence combustion phasing has on engine performance. The advancing *CA50* below 2°CA aTDC causes a drop in *ITE* of about 1.5pp for case A, for H_2 energy share of 25%. However, this needs to be controlled to occur between 3 and 8°CA aTDC, which is the optimal window for *CA50* to maximize performance, based on our prior experience on RCCI combustion. In addition, burn duration also plays a contributing role, wherein a much shorter duration than conventional combustion concepts, results in the

high thermal efficiencies that is characteristic to LTC concepts.

Furthermore, strategies as those discussed in section 3.3 are a first step in showing the modulation of mixture reactivity to control combustion phasing. However, the combined effect of both strategies holds significant potential. Reduction in intake temperature results in increased charge density, and combined with higher share of LRF, produces a greater reduction in specific fuel consumption, CO_2 emissions and improved thermal efficiency at the typically challenging low and partial load operation. The addition of the strategy of mixture strength (λ_{total}) potentially allows for leaner operation with H_2 admixing, a further benefit.

Importantly, the aforementioned strategies enable exploration of higher H_2 energy share (BR>25%) while still satisfying the constraints of PRR_{max} and emissions limits. However, it is worth bearing in mind that safe operation of the system with H_2, especially regarding leakage, is critical. Studies show that up to 20% on volume basis [58] can be blended for immediate use without the need for major modifications to transmission infrastructure and end-consumer installations. However, some regulating bodies, such as the EU [59] restrict this limit further to 10%. Considering splitting the difference, a volume-based limit of 15% translates roughly to 5% on energy basis. Therefore, the resulting performance improvement of a reduction in CH_4 emissions by up to 16%, accompanied by a reduction in overall specific fuel consumption (mass based) by 3.5% can already be observed. On the other hand, BR>25% necessitates care to be taken regarding blow-by and crankcase ventilation, which call for hardware modifications.

The simultaneous exploration of the aforementioned engine operating parameters needs to be conducted on a system level model including all components of the engine to get practical, useable insights. This forms the optimization problem of maximizing engine performance at each load point, within the established constraints. The modelling framework for this is currently under progress, by coupling UVATZ in GT-Power, a commercial 1-D engine system modelling tool [46]. Such a holistic development requires dedicated infrastructure and strategic commitment as foreseen within a portfolio of projects headed by the university of Vaasa which include Clean Propulsion Technologies [7], CASEMATE [60] and DAZE [61].

5. Conclusions

In the context of decarbonising dual-fuel marine gas engines, the present model-based study is conducted via an experimentally validated chemical-kinetics based, fast multizone model. This unique methodology for the first time allows to bridge the gap between fundamental knowledge on combustion kinetics of hydrogen – natural gas – diesel mixtures towards the applied issues of combustion engine control. The established connection is a milestone towards designing feasible hydrogen (H_2) propulsion based on cutting edge dual-fuel engine technology working in low-temperature reactivity-controlled compression ignition (RCCI) mode.

In the context of methodological feasibility, the study draws following conclusions:

- The proposed multizone simulation framework can reproduce all performance and emission indicators of a RCCI engine. The model's predictivity allows for exploring the effects of H_2 admixing, which was efficiently calibrated using limited points from the baseline natural gas (NG) – diesel RCCI experiments.
- All performance indicators can be predicted under 5% error, with trend-wise validity on emissions. The trends with hydrogen are inline with earlier reported, more fundamental works on RCCI combustion.
- Fast simulation times at 3 min, allows extensive exploration of cross-influences of H_2 admixing with three relevant engine control parameters. The expense of 72 cases simulated in this study, under fully converged air-path conditions (6–8 engine cycles each) is unattainable for similar CFD-based studies.

The conclusions of fundamental scientific relevance are as follows:

- H_2 admixing advances combustion phasing at an average rate of 0.3°CA/%H_2. This is a result of the higher reactivity of H_2 wherein a higher concentration of OH and HO_2 in the radical pool causes increased rate of chain branching reactions of the NG – diesel reaction pathway. Notably, the trend is most pronounced with low H_2 concentrations and saturates towards higher admixtures.
- Increasing *overall* mixture *reactivity correspondingly* decreases methane slip by as much as 80% at 25% blending. To this end, H_2 allows more complete combustion of the inner-cylinder zones, that in RCCI remain hardly seeded with diesel fuel.
- At the same time, combustion harshness, quantified by peak pressure rise rate, increases. For operation at mid-load, the durability limit of the engine is surpassed already at 13% H_2 blending. Simultaneously, NO_X emissions rises due to increasing combustion temperature, surpassing EU stage V regulation at 8% H_2 addition.

Incorporating the above phenomenological insights to feasible control strategies enables understanding the full potential of H_2 enriched RCCI concept in terms of emissions and performance. The findings by this study are highlighted in following points:

- Both liquid fuel blending control and intake air thermal management, allow to retain inherent benefits of hydrogen admixing, in terms of methane slip and CO_2 reduction, while mitigating the mentioned PRR/NO_x drawback.
- At the 50% load point, the H_2 energy share was maximized by reducing intake temperature by 12K, thus keeping both PRR and NO_x within the limits of the baseline NG-diesel operation. Alternatively, the high reactivity fuel can be reduced by a rate of 7% to achieve the same goal.
- While neither approaches compromise engine performance, the added benefit of the latter is a potential 1–1.5 pp improvement in indicated efficiency accompanied by a further decrease in GHG emissions by 27%, compared to operation without H_2. Reducing the amount of diesel will face issues with injection moving to ballistic region, rendering both strategies necessary to secure safe operation at H_2 admixtures above 50%.
- The fast UVATZ code, utilized here for proof of concept, can be easily linearized allowing efficient design model-predictive controller to handle the control strategies in real-time. This, forms the main direction of further research along with experimental verification of H2-admixing effects postulated by this study.

The authors declare that they have no known competing financial interests or personal relationships that could have appeared to influence the work reported in this paper.

CRediT authorship contribution statement

Aneesh Vasudev: Writing – original draft, Visualization, Validation, Software, Methodology, Investigation, Funding acquisition, Formal analysis, Conceptualization. **Amir Soleimani:** Writing – original draft, Visualization, Validation, Software, Formal analysis, Data curation. **Jari Hyvönen:** Writing – review & editing, Supervision, Resources. **Maciej Mikulski:** Writing – review & editing, Supervision, Resources, Project administration, Methodology, Funding acquisition, Conceptualization.

Declaration of competing interest

The authors declare the following financial interests/personal relationships which may be considered as potential competing interests:

Aneesh Vasudev reports financial support was provided by Business Finland. Aneesh Vasudev reports financial support was provided by Ella and Georg Ehrnrooth foundation. If there are other authors, they declare that they have no known competing financial interests or personal relationships that could have appeared to influence the work reported in this paper.

Acknowledgements

The work was conducted in the framework of the Clean Propulsion Technologies project [7] with financial support from Business Finland (ref. 38485/31/2020). The authors would also like to acknowledge Ella and Georg Ehrnrooth foundation (17-12898-11) for graciously funding the research. Finally, we appreciate the invaluable contribution of Mr David Wilcox in proofreading our manuscript and providing his expert suggestions on stylistic points.

Appendix A. Supplementary data

Supplementary data to this article can be found online at https://doi.org/10.1016/j.ijhydene.2025.02.152.

References

[1] Hydrogen Insights 2023: an update on the state of the global hydrogen economy, with a deep dive into North America. Belgium: Hydrogen Council, McKinsey & Company; 2023.
[2] Hoffmann J, Sirimanne SN. Review of maritime transport 2017. Geneva, Switzerland: UNCTAD; 2017.
[3] Aakko-Saksa PT, Lehtoranta K, Kuittinen N, Järvinen A, Jalkanen J-P, Johnson K, et al. Reduction in greenhouse gas and other emissions from ship engines: current trends and future options. Prog Energy Combust Sci 2023;94:101055. https://doi.org/10.1016/j.pecs.2022.101055.
[4] Doosje E, Willems F, Baert R. Experimental demonstration of RCCI in heavy-duty engines using diesel and natural gas. SAE International 2014. https://doi.org/10.4271/2014-01-1318.
[5] Hanson R, Ickes A, Wallner T. Comparison of RCCI operation with and without EGR over the full operating map of a heavy-duty diesel engine. USA: SAE 2016. https://doi.org/10.4271/2016-01-0794.
[6] Kokjohn SL, Hanson RM, Splitter DA, Reitz RD. Fuel reactivity controlled compression ignition (RCCI): a pathway to controlled high-efficiency clean combustion. Int J Engine Res 2011;12:209–26. https://doi.org/10.1177/1468087411401548.
[7] Clean Propulsion Technology. Clean Propulsion n.d. https://cleanpropulsion.org/(accessed August 12, 2021).
[8] Niemi S. Intens. University of Vaasa research projects. 2018. https://www.uwasa.fi/fi/tutkimus/hankkeet/intens.
[9] Lehtoranta K, Kuittinen N, Vesala H, Koponen P. Methane emissions from a state-of-the-art LNG-powered vessel. Atmosphere 2023;14. https://doi.org/10.3390/atmos14050825.
[10] Ansari E, Shahbakhti M, Naber J. Optimization of performance and operational cost for a dual mode diesel-natural gas RCCI and diesel combustion engine. Appl Energy 2018;231:549–61. https://doi.org/10.1016/j.apenergy.2018.09.040.
[11] Paykani A, Garcia A, Shahbakhti M, Rahnama P, Reitz RD. Reactivity controlled compression ignition engine: pathways towards commercial viability. Appl Energy 2021;282:116174. https://doi.org/10.1016/j.apenergy.2020.116174.
[12] Paykani A, Kakaee A-H, Rahnama P, Reitz RD. Progress and recent trends in reactivity-controlled compression ignition engines. Int J Engine Res 2016;17:481–524. https://doi.org/10.1177/1468087415593013.
[13] Mikulski M, Balakrishnan PR, Doosje E, Bekdemir C. Variable valve actuation strategies for better efficiency load range and thermal management in an RCCI engine. SAE International; 2018. https://doi.org/10.4271/2018-01-0254.
[14] Guo H, Neill WS. The effect of hydrogen addition on combustion and emission characteristics of an n-heptane fuelled HCCI engine. Int J Hydrogen Energy 2013;38:11429–37. https://doi.org/10.1016/j.ijhydene.2013.06.084.
[15] Rahnama P, Paykani A, Reitz RD. A numerical study of the effects of using hydrogen, reformer gas and nitrogen on combustion, emissions and load limits of a heavy duty natural gas/diesel RCCI engine. Appl Energy 2017;193:182–98. https://doi.org/10.1016/j.apenergy.2017.02.023.
[16] Ramachandran E, Krishnaiah R, Perumal Venkatesan E, Medapati SR, Sabarish R, Khan SA, et al. Experimental studies to reduce usage of fossil fuels and improve green fuels by adopting hydrogen–ammonia–biodiesel as trinary fuel for RCCI engine. ACS Omega 2024;9:741–52. https://doi.org/10.1021/acsomega.3c06327.
[17] Kumar M, Paul A. Comparative evaluation of combustion, performance, exergy and emission characteristics in hydrogen-biodiesel dual fuel engine under RCCI mode. Energy Environ 2024;35:3418–40. https://doi.org/10.1177/0958305X231167467.
[18] Kakoee A, Bakhshan Y, Aval SM, Gharehghani A. An improvement of a lean burning condition of natural gas/diesel RCCI engine with a pre-chamber by using hydrogen. Energy Convers Manag 2018;166:489–99. https://doi.org/10.1016/j.enconman.2018.04.063.
[19] Bazrafshan J, Jazayeri A, Ebrahimi M, Khaleghinia J. The effect of hydrogen addition on a RCCI engine performance fueled with natural GasDiesel fuel at low load range. The Journal of Engine Research 2022;65:60–74.
[20] Kokabi H, Najafi M, Jazayeri SA, Jahanian O. Hydrogen and propane implications for reactivity controlled compression ignition combustion engine running on landfill gas and diesel fuel. Int J Hydrogen Energy 2021;46:31903–15. https://doi.org/10.1016/j.ijhydene.2021.07.050.
[21] Kalsi SS, Subramanian KA. Experimental investigations of effects of hydrogen blended CNG on performance, combustion and emissions characteristics of a biodiesel fueled reactivity controlled compression ignition engine (RCCI). Int J Hydrogen Energy 2017;42:4548–60. https://doi.org/10.1016/j.ijhydene.2016.12.147.
[22] Das S, Debnath BK, Negi S, Das B, Safari S, Reddy BV, et al. A comprehensive review into the effects of different parameters on the hydrogen-added HCCI diesel engine. Energy Sci Eng 2023;11:3928–58. https://doi.org/10.1002/ese3.1559.
[23] Hanafi Gharehlar H, Ebrahimi M, Hosseinzadeh M, Hosseini S. Hydrogen/diesel RCCI engine performance assessment at low load. Int J Hydrogen Energy 2024;58:200–9. https://doi.org/10.1016/j.ijhydene.2024.01.172.
[24] Ekin F, Ozsoysal OA, Arslan H. The effect of using hydrogen at partial load in a diesel-natural gas dual fuel engine. Int J Hydrogen Energy 2022;47:18532–50. https://doi.org/10.1016/j.ijhydene.2022.03.287.
[25] Shudo T, Yamada H. Hydrogen as an ignition-controlling agent for HCCI combustion engine by suppressing the low-temperature oxidation. Int J Hydrogen Energy 2007;32:3066–72. https://doi.org/10.1016/j.ijhydene.2006.12.002.
[26] Salmani Marasht MR, Jazayeri SA, Ebrahimi M. Detailed analysis of a pure hydrogen-fueled dual-fuel engine in terms of performance and greenhouse gas emissions. Alex Eng J 2024;109:250–61. https://doi.org/10.1016/j.aej.2024.08.086.
[27] Sattarzadeh M, Ebrahimi M, Jazayeri SA. Maximum reduction in greenhouse gas emissions by complete replacement of natural gas with pure hydrogen as a sole low reactive fuel in a RCCI engine. Int J Engine Res 2023;24:2677–91. https://doi.org/10.1177/14680874221128353.
[28] Ebrahimi M, Jazayeri SA. Effect of hydrogen addition on RCCI combustion of a heavy duty diesel engine fueled with landfill gas and diesel oil. Int J Hydrogen Energy 2019;44:7607–15. https://doi.org/10.1016/j.ijhydene.2019.02.010.
[29] Chintala V, Subramanian KA. An effort to enhance hydrogen energy share in a compression ignition engine under dual-fuel mode using low temperature combustion strategies. Appl Energy 2015;146:174–83. https://doi.org/10.1016/j.apenergy.2015.01.110.
[30] Duan H, Jia M, Xu Z, Li Y, Xia G. Comprehensive analysis of combustion behaviors of hydrogen (H2)/diesel reactivity-controlled compression ignition (RCCI) in a light-duty diesel engine. Fuel 2023;353:129237. https://doi.org/10.1016/j.fuel.2023.129237.
[31] Karbasi J, Jazayeri SA, Ebrahimi M. Evaluation of significant greenhouse gas emissions reduction using hydrogen fuel in a LFG/Diesel RCCI engine. Journal of Engineering Research 2024:S2307187724000129. https://doi.org/10.1016/j.jer.2024.01.012.
[32] Karthic SV, Senthil Kumar M. Experimental investigations on hydrogen biofueled reactivity controlled compression ignition engine using open ECU. Energy 2021;229:120787. https://doi.org/10.1016/j.energy.2021.120787.
[33] Mohamed Ibrahim M, Ramesh A. Investigations on the effects of intake temperature and charge dilution in a hydrogen fueled HCCI engine. Int J Hydrogen Energy 2014;39:14097–108. https://doi.org/10.1016/j.ijhydene.2014.07.019.
[34] Vasudev A, Kakoee A, Axelsson M, Almani HM, Hyvönen J, Mikulski M. Advancing autonomy of chemical kinetics based multizone models for reactivity controlled compression ignition engines. Energy Convers Manag 2024;312:118562. https://doi.org/10.1016/j.enconman.2024.118562.
[35] Vasudev A, Cafari A, Axelsson M, Mikulski M, Hyvönen J. Towards next generation control-oriented thermo-kinetic model for reactivity controlled compression ignition marine engines. SAE 2022. https://doi.org/10.4271/2022-01-1033.
[36] Storm X, Vasudev A, Shamekhi A-M, Modabberian A, Zenger K, Hyvönen J, et al. Real-time predictive model for reactivity controlled compression ignition marine engines. Control Eng Pract 2023;141:105724. https://doi.org/10.1016/j.conengprac.2023.105724.
[37] Kakoee A, Hunicz J, Mikulski M. Integrated 1D simulation of aftertreatment system and chemistry-based multizone RCCI combustion for optimal performance with methane oxidation catalyst. J Mar Sci Eng 2024;12. https://doi.org/10.3390/jmse12040594.
[38] Vasudev A, Mikulski M, Hyvönen J. Effect of H2 admixture on RCCI combustion dual-fuel marine engines: a model-based study. Proceedings of the 14th international Exergy, energy and environment symposium. 2023. p. 61–5. Turkey.
[39] Wärtsilä 20DF product guide. Vaasa, Finland. WÄRTSILÄ FINLAND Oy; 2024.
[40] Ryan Walker N, Wissink ML, DelVescovo DA, Reitz RD. Natural gas for high load dual-fuel reactivity controlled compression ignition in heavy-duty engines. J Energy Resour Technol 2015;137. https://doi.org/10.1115/1.4030110.
[41] Goodwin DG, Moffat HK, Speth RL. Cantera: an object-oriented software toolkit for chemical kinetics, thermodynamics, and transport processes. Version 2.4.0, https://doi.org/10.5281/zenodo.170284; 2018.
[42] Bozza F, Teodosio L, De Bellis V, Fontanesi S, Iorio A. A refined OD turbulence model to predict tumble and turbulence in SI engines. SAE International Journal of Engines 2019;12:15–30.
[43] Chang J, Güralp O, Filipi Z, Assanis D, Kuo T-W, Najt P, et al. New heat transfer correlation for an HCCI engine derived from measurements of instantaneous

surface heat flux. SAE Transactions, Section 3: Journal of Engines 2004;113:1576–93.
[44] Yao T, Pei Y, Zhong B-J, Som S, Lu T, Luo KH. A compact skeletal mechanism for n-dodecane with optimized semi-global low-temperature chemistry for diesel engine simulations. Fuel 2017;191:339–49. https://doi.org/10.1016/j.fuel.2016.11.083.
[45] Sun Y, Reitz R. Modeling diesel engine NOx and soot reduction with optimized two-stage combustion. SAE International 2006. https://doi.org/10.4271/2006-01-0027.
[46] Kakoee A, Vasudev A, Smulter B, Hyvönen J, Mikulski M. A fully predictive 1-D modelling framework for reactivity-controlled compression ignition engine via chemistry based multi-zone model. SAE International 2023. https://doi.org/10.4271/2023-24-0001.
[47] Cohen SD, Hindmarsh AC, Dubois PF. CVODE, A stiff/nonstiff ODE solver in C. Comput Phys 1996;10:138.
[48] Vasudev A, Mikulski M, Balakrishnan PR, Storm X, Hunicz J. Thermo-kinetic multi-zone modelling of low temperature combustion engines. Prog Energy Combust Sci 2022;91:100998. https://doi.org/10.1016/j.pecs.2022.100998.
[49] De Bellis V, Malfi E, Lanotte A, Fasulo G, Bozza F, Cafari A, et al. Development of a phenomenological model for the description of RCCI combustion in a dual-fuel marine internal combustion engine. Appl Energy 2022;325:119919. https://doi.org/10.1016/j.apenergy.2022.119919.
[50] Voshtani S, Reyhanian M, Ehteram M, Hosseini V. Investigating various effects of reformer gas enrichment on a natural gas-fueled HCCI combustion engine. Int J Hydrogen Energy 2014;39:19799–809. https://doi.org/10.1016/j.ijhydene.2014.09.130.
[51] Reyhanian M, Hosseini V. Various effects of reformer gas enrichment on natural-gas, iso-octane and normal-heptane HCCI combustion using artificial inert species method. Energy Convers Manag 2018;159:7–19. https://doi.org/10.1016/j.enconman.2017.12.074.
[52] Shao Z, Dallmann T. European Stage V non-road emission standards. Berlin: The International Council on Clean Transportation; 2016.
[53] Solomon S, Qin D, Manning M, Chen Z, Marquis M, Averyt KB, et al. Contribution of working group I to the fourth assessment report of the intergovernmental panel on climate change, 2007. Cambridge: Intergovernmental Panel on Climate Change (IPCC); 2007.
[54] Troe J. The thermal dissociation/recombination reaction of hydrogen peroxide H2O2(+M)⇔2OH(+M) III.: analysis and representation of the temperature and pressure dependence over wide ranges. Combust Flame 2011;158:594–601. https://doi.org/10.1016/j.combustflame.2010.08.013.
[55] Burke MP, Chaos M, Ju Y, Dryer FL, Klippenstein SJ. Comprehensive H2/O2 kinetic model for high-pressure combustion. Int J Chem Kinet 2012;44:444–74. https://doi.org/10.1002/kin.20603.
[56] Hashemi H, Christensen JM, Gersen S, Levinsky H, Klippenstein SJ, Glarborg P. High-pressure oxidation of methane. Combust Flame 2016;172:349–64. https://doi.org/10.1016/j.combustflame.2016.07.016.
[57] Kakoee A, Mikulski M, Vasudev A, Axelsson M, Hyvönen J, Salahi MM, et al. Start of injection influence on in-cylinder fuel distribution, engine performance and emission characteristic in a RCCI marine engine. Energies 2024;17. https://doi.org/10.3390/en17102370.
[58] Di Sciullo Jones A, Kai-Hsiang (Jerry) Y. Hydrogen use in natural gas pipeline. United States: UL Solutions; 2023.
[59] Kanaellopoulos K, Busch S, De Felice M, Giaccaria S, Costescu A. Bleding hydrogen from electrolysis into the European gas grid. Luxembourg: Publications Office of the European Union; 2022.
[60] Casemate - computationally aided systems engineering for marine advanced technology for the environment. University of Vaasa; 2023. https://www.uwasa.fi/fi/tutkimus/hankkeet/casemate-computationally-aided-systems-engineering-marine-advanced-technology. [Accessed 12 August 2021].
[61] DAZE - Data Analytics for Zero Emission Marine. University of Vaasa; 2023. https://www.uwasa.fi/en/research/projects/daze-data-analytics-zero-emission-marine. [Accessed 12 August 2021].